

NONLINEAR OPTICAL PHENOMENA https://doi.org/10.1070/QEL16764

Parametric stimulated Raman scattering in barium nitrate crystals

V.S. Gorelik, A.V. Skrabatun, V.A. Orlovich, Yu.P. Voinov, A.I. Vodchits, A.Yu. Pyatyshev

Abstract. **The spectra of multifrequency parametric stimulated Raman scattering in a barium nitrate single crystal is investigated. When this single crystal is excited by ultrashort (80 ps) YAG:Nd^{3+} laser pulses with a wavelength of 1064 nm, a frequency comb of eight anti-Stokes components is observed in the visible spectral range. The Raman satellites are due to the totally symmetric vibrational modes of barium nitrate single crystal. The frequencies of the corresponding Raman Stokes components in the IR range (from 1193 to 9662 nm) are calculated. The results of the study open the way to form an array of laser frequencies from the IR to green spectral range with a period of 1047 cm^{-1}.**

Keywords: *barium nitrate, stimulated Raman scattering, parametric process, opalescence, crystal, spontaneous Raman scattering, group theory.*

1. Introduction

Stimulated Raman scattering (SRS) is an efficient method of nonlinear optical conversion of laser frequency. The results of studying this phenomenon were analysed in reviews [1, 2]. It is known [3] that an increase in the excitation radiation intensity leads also to manifestation of four-wave parametric processes in the spectra of SRS-active media. As a result, multifrequency parametric SRS occurs, whose spectrum exhibits numerous Stokes and anti-Stokes satellites. A theoretical analysis of four-wave parametric processes and results of calculating the wave-matching conditions were reported in [4–6]. Axial generation of anti-Stokes waves under multifrequency SRS was also observed in [7]. It was explained within the model with spatially limited phase locking for parametrically coupled waves.

V.S. Gorelik, A.V. Skrabatun P.N. Lebedev Physical Institute, Russian Academy of Sciences, Leninskii prosp. 53, 119991 Moscow, Russia; Bauman Moscow State Technical University, Vtoraya Baumanskaya ul. 5, stroenie 1, 107005 Moscow, Russia; e-mail: gorelikvs@lebedev.ru, alskrabatun@mail.ru;
V.A. Orlovich, A.I. Vodchits B.I. Stepanov Institute of Physics, National Academy of Sciences of Belarus, prosp. Nezavisimosti 68, 220072 Minsk, Belarus;
Yu.P. Voinov P.N. Lebedev Physical Institute, Russian Academy of Sciences, Leninskii prosp. 53, 119991 Moscow, Russia;
A.Yu. Pyatyshev Bauman Moscow State Technical University, Vtoraya Baumanskaya ul. 5, stroenie 1, 107005 Moscow, Russia; JSC "RPC 'Istok' named after Shokin", ul. Vokzal'naya 2a, 141190 Fryazino, Moscow region, Russia; e-mail: jb_valensia@mail.ru

Received 26 June 2018; revision received 22 November 2018
Kvantovaya Elektronika **49** (3) 231–236 (2019)
Translated by Yu.P. Sin'kov

Currently, multifrequency parametric SRS is used to make laser frequency red- or blue-shifted. This approach stimulates the search for new solid-state Raman-active materials and study of their optical properties in order to design compact, reliable, and efficient laser frequency converters. Barium nitrate crystals are one of the most promising solid-state Raman-active materials [8] to this end.

Physical, chemical, and optical properties of $Ba(NO_3)_2$ crystals were thoroughly studied in [9]. The Raman gain of barium nitrate single crystal is 11 cm GW^{-1} under pumping by 1064-nm laser radiation; this value is record for the artificial crystals known to date. At the excitation wavelength of 532 nm, this coefficient is 47 cm GW^{-1}. The maximum SRS conversion coefficient in $Ba(NO_3)_2$ crystal is 40% for the first Stokes component and 25% for the second component under single-pass pumping. Barium nitrate single crystal has a high fracture threshold; it is very soft and plastic and has a low thermal conductivity [9–14]. Solid-state SRS media are often applied for frequency conversion of Nd laser radiation into the eye-safe spectral region [15–18]. Barium nitrate single crystals are one of the best materials that are applied for laser frequency shift using the SRS effect, including femtosecond excitation [19]. It was established in [9] that the $Ba(NO_3)_2$ crystal has a positive real part of nonlinear susceptibility, which leads to self-focusing when irradiating this crystal by picosecond (35±5 ps) pulses of YAG:Nd^{3+} laser (λ = 1064 nm) with a repetition frequency of 10 Hz. The use of lasers in different SRS excitation regimes showed that the SRS quantum conversion efficiency in $Ba(NO_3)_2$ crystals can be raised to 80% [20].

Eichler et al. [21] observed four anti-Stokes components upon SRS excitation in barium nitrate crystals by a YAG:Nd^{3+} laser, using biharmonic pumping at λ_1 = 1064 nm and λ_2 = 532 nm, with pulse durations of 120 and 80 ps, respectively. The angular distribution of Stokes–anti-Stokes rings on an opaque screen during four-wave mixing upon excitation of secondary radiation by the second harmonic of the YAG:Nd^{3+} laser with λ = 532 nm was reported in [22]. Parametric SRS with the formation of many Raman satellites was also observed upon picosecond SRS excitation in other crystals (BaF_2 [23], $CaCO_3$ [24], $LuVO_4$ [25]) and in $Ca(NO_3)_2$:KNO_3 glasses [26]. Intense multifrequency scattering was revealed under resonance-excitation conditions in sodium nitrite crystals using a pulsed nitrogen laser (λ = 337 nm) [27].

The crystalline structure of barium nitrate is a subject of numerous studies [28–33], the main purpose of which was to prove or disprove the presence of centre of symmetry in this crystal. A simulation of the barium nitrate crystal structure and theoretical calculation of the frequencies of IR- and Raman-active spectral components were performed

using the exchange-correlation functional in [30]. $Ba(NO_3)_2$ crystals have been repeatedly investigated by IR spectroscopy [9, 15, 30, 34, 35] and spontaneous Raman scattering (RS) and SRS [9, 21, 35–38].

The purpose of this study was to gain more detailed information about the spontaneous Raman scattering spectra of barium nitrate single crystals and the characteristics of multifrequency parametric SRS in this crystal upon picosecond IR excitation by YAG:Nd^{3+} laser radiation with $\lambda = 1064$ nm. The conditions for generating a maximally possible number of Raman satellites at parametric SRS in a $Ba(NO_3)_2$ single crystal were investigated.

2. Theoretical part

It was found in [2] that the parametric coupling of SRS components in liquid benzene leads to self-supporting conical generation of anti-Stokes waves. We interpreted this finding proceeding from the degenerate four-wave mixing between the laser (wave vector $\boldsymbol{k}_P$), Stokes (wave vector $\boldsymbol{k}_S$), and anti-Stokes (wave vector $\boldsymbol{k}_A$) waves, provided that the vector matching condition is satisfied: $2\boldsymbol{k}_P = \boldsymbol{k}_S + \boldsymbol{k}_A$. The four-wave mixing involves two laser pumping photons with identical frequencies, one photon of the first Stokes component, and one photon of the first anti-Stokes component. The energy conservation law for this four-wave mixing has the form $2\hbar\omega_P = \hbar\omega_S + \hbar\omega_A$. According to [39], simultaneous generation of multiple anti-Stokes satellites and only one Stokes component may occur: $\boldsymbol{k}_P + \boldsymbol{k}_A^{(n-1)} = \boldsymbol{k}_S^{(1)} + \boldsymbol{k}_A^{(n)}$ $(n = 2, ...)$. At higher laser pumping intensities, when SRS leads to generation of not only the first but also higher $(n > 1)$ Stokes SRS components, the matching condition was determined in [4] for nondegenerate four-wave mixing: $\boldsymbol{k}^{(n)} + \boldsymbol{k}^{(n+1)} = \boldsymbol{k}^{(n-1)} + \boldsymbol{k}^{(n+2)}$. Other Raman processes of generation of higher Stokes–anti-Stokes satellites may also occur, for example, $2\hbar\omega_P = \hbar\omega_S^{(n)} + \hbar\omega_A^{(n)}$.

The model describing the collinear (along the z axis) multifrequency parametric SRS with partially degenerate four-wave coupling is based on the system of equations for slowly varying complex amplitudes of the Stokes (E_S) and anti-Stokes (E_A) waves and the laser pump wave (E_P) [4, 6]:

$$\begin{aligned}
\frac{dE_S}{dz} &= g_S[|E_P|^2 E_S + E_P^2 E_A^* \exp(i\Delta kz)],\\
\frac{dE_A}{dz} &= -g_A[|E_P|^2 E_A + E_P^2 E_S^* \exp(i\Delta kz)], \qquad (1)\\
\frac{dE_P}{dz} &= g_P[|E_A|^2 E_P - E_P|E_A|^2].
\end{aligned}$$

Here, g_S, g_A, and g_P are the gains of the corresponding waves at SRS; $\Delta k = 2k_P - k_S - k_A$ is the wave mismatch of four-wave mixing; and k_S, k_A, and k_P are the wave numbers of the corresponding waves. The Stokes–anti-Stokes parametric coupling is described by the last terms of the first and second equations of system (1). The other terms in (1) describe the wave amplification at SRS conversion from the previous component (positive terms) and the wave depletion at SRS conversion into the next component (negative terms). Equations (1) allow one to estimate in the first approximation the relationship between the magnitudes of electric fields of laser pumping and the Stokes and anti-Stokes components of parametric SRS.

The $Ba(NO_3)_2$ crystal has a cubic point symmetry group. The unit-cell parameter is $a = 8.11$ Å, and the number of structural units per primitive cell is four [9]. The density of crystalline barium nitrate is 3.24 g cm^{-3}, and its melting temperature is 592 °C. The solubility of $Ba(NO_3)_2$ is fairly low: 8.7 g in 100 mL water at room temperature. The isobaric specific heat C_p at 298 °C is 151.6 J mol^{-1}. The thermal conductivity of barium nitrate single crystals varies from 3.1 W m^{-1} K^{-1} at 100 °C to 1.17 W m^{-1} K^{-1} at 25 °C and 0.92 W m^{-1} K^{-1} at temperatures above 100 °C. Barium nitrate crystals are transparent in a wide spectral range, including visible and near-IR (from 350 to 1800 nm) [9]. The refractive index of barium nitrate is set by the relation $n(\lambda^2) = 2.4069 + 0.01992/(\lambda^2 - 0.03773) - 0.006166\lambda^2$ [40], where λ is the light wavelength in μm.

Nitrate ions in barium nitrate crystals occupy the site with a symmetry C_3. Barium cations occupy the site S_6 for the T_h^6 group and the site with a symmetry C_3 for the T^4 group. Since the primitive cell contains eight nitrate ions, each mode of nitrate ions can be coupled in eight different ways. Cation pairs are coupled in four different ways [22–25]. The unperturbed negative nitrate ion NO_3^- (D_{3h} symmetry) generates the following internal vibrations: $\nu_1(A_1')$ (Raman-active mode with an energy of 1047 cm^{-1}), $\nu_2(A_2'')$ (IR-active mode with an energy of ~820 cm^{-1}), and $\nu_3(E')$ и $\nu_4(E'')$ (Raman- and IR-active vibrations with energies of 1400 and 730 cm^{-1}, respectively) [9].

To analyse in more detail the vibrational spectrum of $Ba(NO_3)_2$ single crystal, we performed a group-theoretical analysis of its modes by the site-symmetry method [41]. The results of the analysis for the centrosymmetric (group T_h^6) and noncentrosymmetric (group T^4) structures are listed in Tables 1 and 2, respectively.

The representation T_{opt} contains the full spectrum of optical vibrations of barium nitrate crystal, which can be decomposed into components: $T_{opt} = T_{tr} + T_{lib} + T_{in}$, where T_{tr} corresponds to translational lattice modes (translational vibrations of the Ba atom), T_{lib} corresponds to librations

Table 1. Results of group-theoretical analysis of the barium nitrate crystal belonging to the symmetry space group T_h^6.

Representation	Classification of vibrations	Number of Raman-active modes
T_{opt}	$4A_g(RS) + 4E_g(RS) + 12F_g(RS) + 5A_u + 5E_u + 14F_u(IR)$	20
T_{tr}	$A_g(RS) + E_g(RS) + 3F_g(RS) + 2A_u + 2E_u + 5F_u(IR)$	5
T_{lib}	$A_g(RS) + E_g(RS) + 3F_g(RS) + A_u + E_u + 3F_u(IR)$	5
T_{in}	$2A_g(RS) + 2E_g(RS) + 6F_g(RS) + 2A_u + 2E_u + 6F_u(IR)$	10

Table 2. Results of group-theoretical analysis of the barium nitrate crystal belonging to the symmetry space group T^4.

Representation	Classification of vibrations	Number of Raman-active modes
T_{opt}	$9A(RS) + 9E(RS) + 26F(IR, RS)$	44
T_{tr}	$3A(RS) + 3E(RS) + 8F(IR, RS)$	14
T_{lib}	$2A(RS) + 2E(RS) + 6F(IR, RS)$	10
T_{in}	$4A(RS) + 4E(RS) + 12F(IR, RS)$	20

(rockings) of the NO_3^- group, and T_{in} corresponds to the intramolecular (internal) vibrations of the NO_3^- group. According to the selection rules [41], the IR absorption is allowed for the triply degenerate vibration $V = F_u$ (for the T_h^6 group) or $V = F$ (for the T^4 group) and Raman scattering is allowed for the symmetric vibrations $[V]^2 = A_g + E_g + F_g$ (for the T_h^6 group) or $[V]^2 = A + E + F$ (for the T^4 group). The activity of modes (IR or Raman) is indicated in parentheses in Tables 1 and 2. Thus, the Raman spectrum should contain 10 lines for the T_h^6 group (Table 1) or 24 lines for the T^4 group (Table 2), corresponding to the lattice modes lying in low-frequency spectral region. High-frequency vibrations, corresponding to the internal vibrations of the nitrate group, should manifest themselves in the form of 10 or 20 bands (for the T_h^6 and T^4 groups, respectively).

3. Experimental

Spontaneous Raman scattering spectra were excited and recorded on an experimental setup (see schematic in Fig. 1). The excitation source was a laser (*1*) with a wavelength $\lambda = 785$ nm and power of 200 mW. The laser beam was introduced into the first optical fibre (*2*) and a probe (*3*). A lens (*5*) focused the beam onto a sample (*6*). The Raman signal formed in the sample entered the second optical fibre (*8*), was filtered in a focusing system (*9*) using a photonic crystal (*11*), and arrived at the input of a mini-spectrometer (*13*) with a multielement detector. A computer (*14*) performed digital processing and storage of Raman spectra. The spectral resolution was 1 cm^{-1}.

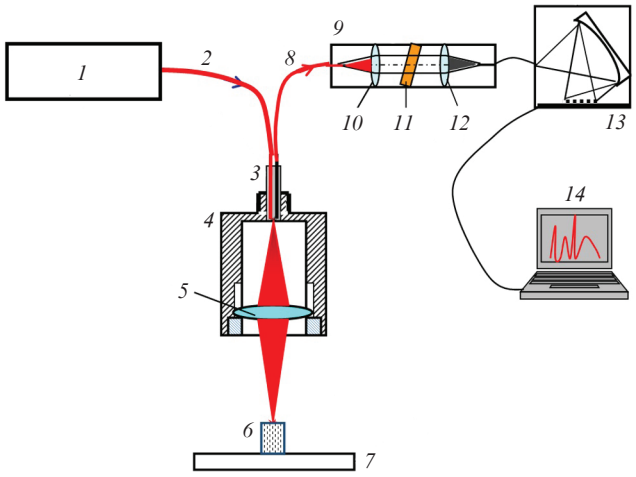

Figure 1. Schematic of the experimental setup for observing spontaneous Raman scattering:
(*1*) laser; (*2*, *8*) first and second optical fibres; (*3*) probe; (*4*) housing; (*5*, *10*, *12*) lenses; (*6*) single crystal; (*7*) substrate; (*9*) focuser; (*11*) photonic crystal for suppressing excitation radiation; (*13*) minispectrometer; (*14*) computer.

The excitation source for multifrequency parametric SRS was a YAG:Nd^{3+} laser with a wavelength $\lambda = 1.064$ μm, which generated 80-ps pulses with a repetition rate of 20 Hz. The maximum energy and power per pulse reached 20 mJ and 0.3 GW, respectively. When focusing the laser beam in the insulators under study, its maximum intensity was ~1 TW cm^{-2}. The sample of barium nitrate single crystal was a rectangular parallelepiped 100 mm long.

Figure 2 shows a schematic of the experimental setup for observing multifrequency parametric SRS. Radiation from a source (*1*), having passed through a semitransparent plate (*2*) and a quartz lens (*3*), arrived at a sample (*6*) (barium nitrate single crystal). The scattered radiation from crystal, transmitted through the focusing lens (*3*) and optical fibre (*7*), arrived to a FSD-8 spectrometer (*4*), connected to a computer (*5*). To detect multifrequency SRS radiation in the 'backward' direction after the semitransparent plate (*2*), an additional quartz lens (*3*), a fibre (*7*), a spectrometer (*4*), and a computer (*5*) were applied. The FSD-8 spectrometer, equipped with a multielement detector, made it possible to record spectra in a wide range (200–1000 nm), with exposures from 100 μs to 32 s. The spectral resolution was ~1 nm.

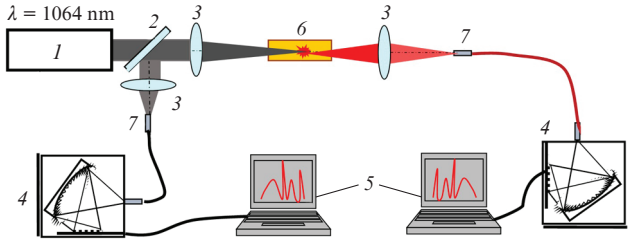

Figure 2. Schematic of the experimental setup for observing anti-Stokes SRS:
(*1*) YAG:Nd^{3+} laser; (*2*) semitransparent plate; (*3*) focusing lens; (*4*) spectrometers; (*5*) computers; (*6*) sample; (*7*) fibre.

Figure 3 shows a schematic of the setup for recording the angular distribution of anti-Stokes rings on an opaque screen. The distance between the barium nitrate crystal and screen is 30 cm.

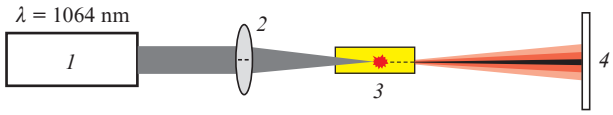

Figure 3. Schematic of the experimental setup for observing anti-Stokes SRS on an opaque screen:
(*1*) YAG:Nd^{3+} laser; (*2*) focusing lens; (*3*) sample; (*4*) opaque screen.

4. Experimental results and discussion

Figure 4 shows spontaneous Raman scattering spectra of barium nitrate crystal, recorded upon excitation by a laser beam with $\lambda = 785$ nm. The spectra in Figs 4a and 4b were obtained with exposures $t = 200$ and 400 s, respectively.

The spontaneous Raman scattering spectra of barium nitrate single crystal consist of a small number of very narrow lines. At a short exposure, one can observe a doublet in the range of 130–145 cm^{-1}. At a longer exposure, splitting of low-frequency lines is absent, but an additional weak peak arises near $\nu = 1638$ cm^{-1}. Table 3 contains Raman shifts of the lines presented in Fig. 4, with their assignment according to their symmetry types for different space groups.

Using the values of frequency shifts (Table 3) and the results of [9, 33, 34], the Raman satellites were assigned to the vibration modes allowed in Raman scattering according to the selection rules. The low-frequency satellites correspond

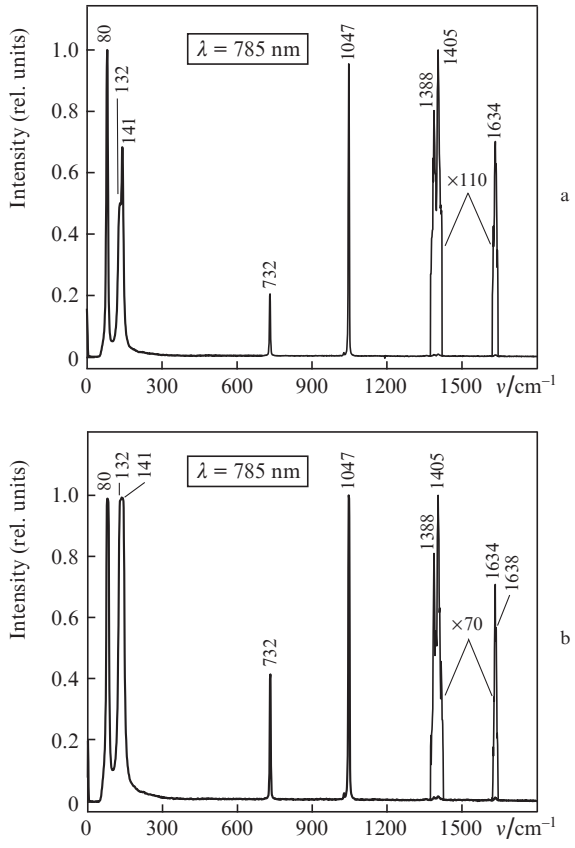

Figure 4. Spontaneous Raman scattering spectra of a barium nitrate crystal, recorded with exposures of (a) 200 and (b) 400 s.

Table 3. Vibration frequencies and their assignment according to symmetry types in a room-temperature Raman spectrum of barium nitrate.

Raman shift/ cm^{-1}	Vibration symmetry type T_h^6	Vibration symmetry type T^4	Vibration type
80	F_g	F	Lattice
132	F_g	F	
141	E_g	E	
732	E_g, F_g	F	Internal
1047	A_g	A, F	
1388	F_g	E	
1405	F_g	E	
1634 1638	A_g, F_g	A, F	

to the lattice vibrations of barium nitrate crystal. The low-frequency spectral components and the line at $\nu = 1047$ cm^{-1} have the highest intensity in the scattered radiation spectrum. The narrow high-frequency bands are due to the internal vibrations of the nitrate group. The half-width of the strongest line (at $\nu = 1047$ cm^{-1}) in the spontaneous Raman scattering spectrum was 2.5 cm^{-1}.

Figure 5 shows the spectra of anti-Stokes multifrequency parametric SRS in barium nitrate single crystal, obtained upon excitation by YAG:Nd^{3+} laser radiation with $\lambda = 1064$ nm.

The spectrum contains many Raman satellites (Fig. 5), located in a wide (near-IR and visible) range. The corresponding wavelengths, frequencies, and spectral distances between Raman satellites in the SRS spectra are listed in Table 4.

According to Fig. 5 and the data of Table 4, the multi-frequency parametric SRS spectrum of a barium nitrate crystal, recorded under pulsed-periodic picosecond pumping by a YAG:Nd^{3+} laser, contains eight anti-Stokes (AS) components, shifted with respect to each other by $\nu = 1047$ cm^{-1}

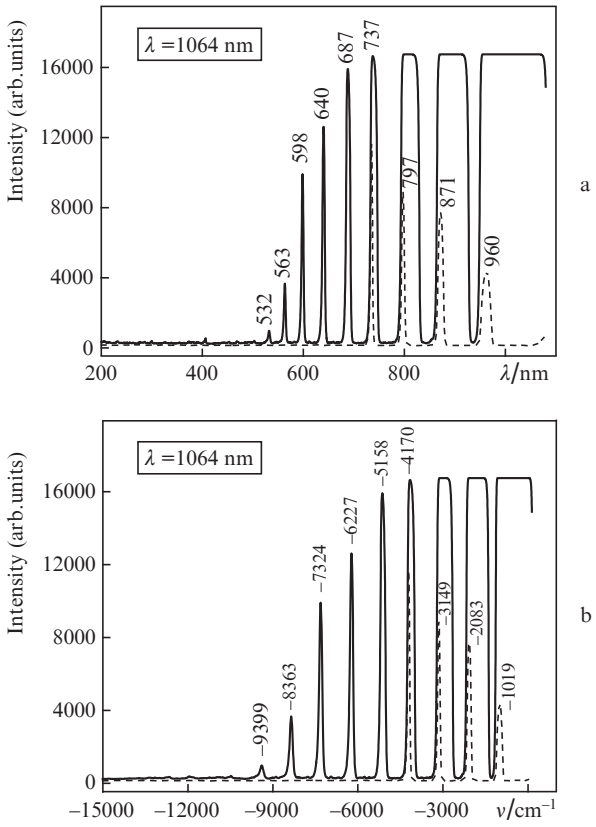

Figure 5. Spectra of anti-Stokes parametric SRS in a barium nitrate crystal in dependence on (a) wavelength λ and (b) frequency ν. The dashed curves are the spectra recorded with a shorter exposure.

Table 4. Parameters of observed anti-Stokes (AS) and calculated Stokes (S) SRS components. The error in measuring frequencies with allowance for the spectrometer resolution is 50 cm^{-1}.

Wavelength/nm	Frequency/cm^{-1}	Frequency shift/cm^{-1}	Line
532	18797	1036	$2\nu_0$
563	17761	1039	AS8
598	16722	1097	AS7
640	15625	1069	AS6
687	14556	988	AS5
737	13568	1021	AS4
797	12547	1066	AS3
871	11481	1064	AS2
960	10417	1019	AS1
1064	9398	–	ν_0
1193	8379	1019	S1
1367	7315	1064	S2
1600	6249	1066	S3
1913	5228	1021	S4
2358	4240	988	S5
3154	3171	1069	S6
4822	2074	1097	S7
9662	1035	1039	S8

(with allowance for the measurement error of ±50 cm^{-1}). According to [9, 22, 35–38], the observed frequency shift is consistent with the spontaneous Raman scattering data and the the SRS spectral data for the crystal under consideration. This frequency shift corresponds to totally symmetric internal vibrations of NO_3^- nitrate ions.

When studying the multifrequency parametric SRS spectra, one would expect each anti-Stokes component (see Fig. 5) to correspond to the Stokes (S) satellite in the IR spectral region, which cannot be recorded by the spectrometer in use. Table 4 contains calculated (in correspondence with the shifts of anti-Stokes components) frequencies and wavelengths of the corresponding Stokes components. The barium nitrate crystal is characterised by strong absorption of mid-IR radiation with wavelengths above 1.8 μm [22]. Thus, the fourth- and higher order Stokes components arising in the spectrum should be significantly weakened. As a whole, upon excitation of multifrequency SRS in a barium nitrate crystal by radiation with $\lambda = 1064$ nm, the SRS spectrum consists of eight anti-Stokes components and several Stokes satellites, which lie in the crystal transparency window.

Note also that, as can be seen in Fig. 5, there is a weak line at the wavelength of second optical harmonic ($\lambda = 532$ nm) of excitation radiation. This line cannot be interpreted as the ninth anti-Stokes component, because its frequency is $\nu = \nu_0 + 9 \times 1047 = 18821$ cm^{-1}, which exceeds the laser overtone frequency $2\nu_0 = 18796$ cm^{-1}. Thus, the narrow line observed at the second-harmonic frequency indicates the absence of centre of symmetry in the barium nitrate crystal. Hence, this crystal is characterised by noncentrosymmetric symmetry space group, i.e., T^4.

Figure 3 shows schematically the observed angular intensity distribution for the anti-Stokes components of multifrequency parametric SRS in a barium nitrate single crystal. One can see that anti-Stokes components are present in the form of rings. The largest deviation angle of coloured ring from the axis of barium nitrate single crystal is ∼1°, a value corresponding to the red anti-Stokes component.

5. Conclusions

We recorded detailed spontaneous Raman scattering spectra of barium nitrate crystal using a laser with $\lambda = 785$ nm as an excitation source. Multifrequency parametric light scattering was observed when exciting SRS in a $Ba(NO_3)_2$ crystal by a picosecond pulsed-periodic $YAG:Nd^{3+}$ laser with $\lambda = 1064$ nm. Eight anti-Stokes satellites, which are due to totally symmetric modes with a frequency shift of 1047 cm^{-1}, were recorded in the spectrum. The position of possible Stokes satellite in the IR region was calculated for each anti-Stokes component. Thus, there arises a possibility of forming a laser frequency array in a wide spectral range: from IR to green. SRS anti-Stokes satellites were characterised by angular distribution in the form of rings, corresponding to different components. The results of the study are interesting for developing the theory of SRS parametric processes in crystals under conditions of strong photon–phonon interaction; they have also applied importance for designing efficient laser sources operating in different spectral ranges.

Acknowledgements. This work was supported by the Russian Foundation for Basic Research (Grant Nos 18-02-00181 and 18-32-00259).

References

1. Shen Y.R. *The Principles of Nonlinear Optics* (New York: Wiley, 1984; Moscow: Nauka, 1989).
2. Blombergen N. *Usp. Fiz. Nauk*, **97**, 307 (1969).
3. Butylkin V.S., Kaplan A.E., Khronopulo Yu.G., Yakubovich E.I. *Rezonansnye vzaimodeistviya sveta s veshchestvom* (Resonance Interactions of Light with Matter) (Moscow: Nauka, 1977).
4. Smetanin S.N., Basiev T.T. *Quantum Electron.*, **42**, 224 (2012) [*Kvantovaya Elektron.*, **42**, 224 (2012)].
5. Smetanin S.N. *Quantum Electron.*, **44**, 1012 (2014) [*Kvantovaya Elektron.*, **44**, 1012 (2014)].
6. Basiev T.T., Smetanin S.N., Shurygin A.S., Fedin A.V. *Phys. Usp.*, **53**, 611 (2010) [*Usp. Fiz. Nauk*, **180**, 639 (2010)].
7. Butylkin V.S. et al. *JETP Lett.*, **17**, 285 (1973) [*Pis'ma Zh. Eksp. Teor. Fiz.*, **17**, 400 (1973)].
8. Basiev T.T., Osiko V.V., Prokhorov A.M., Dianov E.M. *Top. Appl. Phys.*, **89**, 459 (2003).
9. Zverev P.G., Basiev T.T., Osiko V.V., Kulkov A.M., Voitsekhovskii V.N., Yakobson V.E. *Opt. Mater.*, **11**, 315 (1999).
10. Eremenko A.S., Karpukhin S.N., Stepanov A.I. *Sov. J. Quantum Electron.*, **10**, 113 (1980) [*Kvantovaya Elektron.*, **7**, 196 (1980)].
11. Karpukhin S.N., Stepanov A.I. *Sov. J. Quantum Electron.*, **16**, 1927 (1986) [*Kvantovaya Elektron.*, **13**, 1572 (1986)].
12. Vitsinskii S.A., Isakov V.K., Karpukhin S.N., Lovchii I.L. *Quantum Electron.*, **23**, 1001 (1993) [*Kvantovaya Elektron.*, **20**, 1155 (1993)].
13. Karpukhin S.N., Yashin V.E. *Sov. J. Quantum Electron.*, **14**, 1337 (1984) [*Kvantovaya Elektron.*, **11**, 1992 (1984)].
14. Voitsekhovskii V.N., Karpukhin S.N., Yakobson V.E. *Opt. Zhurn.*, **LI**, 30 (1995).
15. Zverev P.G., Basiev T.T., Prokhorov A.M. *Opt. Mater.*, **11**, 335 (1999).
16. Orlovich V.A., Apanasevich P.A., Batishche S.A., Belyi V.N., Bui A.A., Grabchikov A.S., Kazak N.S., Kachinskii A.V. *J. Opt. Technol.*, **67**, 984 (2000).
17. Apanasevich P.A., Batishche S.A., Grabchikov A.S., Kuz'muk A.A., Lisinetskii V.A., Orlovich V.A., Tatur G.A., Chulkov R.V. *J. Appl. Spectrosc.*, **73**, 371 (2006).
18. Lisinetskii V.A., Grabtchikov A.S., Khodasevich I.A., Eichler H.J., Orlovich V.A. *Opt. Commun.*, **272**, 509 (2007).
19. Buganov O.V., Grabtchikov A.S., Malakhov Y.I., Popov Y.M., Orlovich V.A., Tikhomirov S.A. *Laser Phys. Lett.*, **9**, 786 (2012).
20. Basiev T.T., Voitsekhovskii V.N., Zverev P.G., Karpushko F.V., Lyubimov A.V., Mirov S.B., Morozov V.P., Mochalov I.V., Pavlyuk A.A., Sinitsyn G.V., Yakobson V.E. *Sov. J. Quantum Electron.*, **17**, 1560 (1987) [*Kvantovaya Elektron.*, **14**, 2452 (1987)].
21. Eichler H.J., Gad G.M.A., Kaminskii A.A., Rhee H. *J. Zhejiang Univ. Sci.*, **4**, 241 (2003).
22. Zverev P.G., Murray J.T., Powell R.C., Reeves R.J., Basiev T.T. *Opt. Commun.*, **97**, 59 (1993).
23. Kaminskii A.A., Rhee H., Eichler H.J., Bohatý L., Becker P., Takaichi K. *Laser Phys. Lett.*, **5**, 304 (2008).
24. Smetanin S.N., Jelinek M., Kubecek V., Jelinkova H. *Laser Phys. Lett.*, **12**, 095403 (2015).
25. Kaminskii A.A., Rhee H., Eichler H.J., Ueda K., Oka K., Shibata H. *Appl. Phys. B*, **93**, 865 (2008).
26. Burkhalter R., Trusch B., Franz P., Kaminskii A.A., Eichler H.J., Hulliger J.J. *Mater. Chem.*, **11**, 3211 (2001).
27. Gorelik V.S., Lepnev L.S., Pyatyshev A.Yu., Skrabatun A.V. *Neorg. Mater.*, **53**, 49 (2017).
28. Bon A.M., Benoit C., Giordano J.P. *Stat. Sol.*, **78**, 453 (1966).
29. Zhuravlev Yu.N., Korabel'nikov D.V. *Russ. Phys. J.*, **60**, 149 (2017).
30. Zhuravlev Yu.N., Korabel'nikov D.V. *Opt. Spectrosc.*, **122**, 929 (2017) [*Opt. Spektrosk.*, **122**, 972 (2017)].
31. Brooker M.H. *J. Sol. State Chem.*, **28**, 29 (1979).
32. Nowotny H., Heger G. *Acta Crystallogr.*, **39**, 952 (1983).
33. Schutte C.J.H. *Z. Kristallogr.*, **126**, 397 (1968).
34. Brooker M.H., Irish D.E., Boyd G.E. *J. Chem. Phys.*, **53**, 1083 (1970).
35. Lisinetskii V.A., Grabtchikov A.S., Khodasevich I.A., Eichler H.J., Orlovich V.A. *Opt. Commun.*, **272**, 509 (2007).

36. Vodchits A.I., Busko D.N., Orlovich V.A., Lisinetskii V.A., Grabtchikov A.S., Apanasevich P.A., Kiefer W., Eichler H.J., Turpin P.Y. *Opt. Commun*., **272**, 467 (2007).
37. Tandel Vanish H., Patel I.B., Pillai Anil S. *Intern. J. Research Cult. Soc*., **1**, 87 (2017).
38. Apanasevich P.A., Batishche S.A., Grabchikov A.S., Kuz'muk A.A., Lisinetskii V.A., Orlovich V.A., Tatur G.A., Chulkov R.V. *J. Appl. Spectrosc*., **73**, 371 (2006).
39. Chiao R.Y., Townes C.H., Stoicheff B.P. *Phys. Rev. Lett*., **12**, 592 (1964).
40. Zverev P.G., Jia W., Liu H., Basiev T.T. *Opt. Lett*., **20**, 2378 (1995).
41. Zhizhin G.N., Mavrin B.N., Shabanov V.F. *Opticheskie kolebatel'nye spektry kristallov* (Optical Vibrational Spectra of Crystals) (Moscow: Nauka, 1984).